Architecturing Carbon Nanotube-based Flexible Solid State Supercapacitor

K. Adu*, D. Ma**, R. Rajagopalan*** and C. Randall****

*Penn State Altoona, PA, USA, cxa269@psu.edu
**Penn Sate University Park, PA, USA, dom5191@psu.edu
***Penn Sate University Park, PA, USA, rur12@psu.edu
****Penn Sate University Park, PA, USA, car4@psu.edu

ABSTRACT

We report preliminary investigation of an all-solid-state electrochemical double layer capacitor using single wall carbon nanotube electrodes and polymer electrolyte. Binder free single walled carbon nanotubes were self-assembled to form a highly dense 20 μm thick carbon nanotube electrode to be used in electrochemical capacitors. Fabrication of symmetric nanotube capacitors using these electrodes and highly ionically conducting polyvinyl alcohol based hydrogel membranes soaked in aqueous sulfuric acid resulted in a capacitor with power density as high as 1040 KW/kg based on mass of both the electrodes. The time constant of the assembled capacitor was ~ 15 ms and was dependent on the concentration of sulfuric acid. The capacitors showed no degradation in performance even after 10,000 cycles. The charge/discharge measurements at temperatures from 20 ^{o}C to 80 ^{o}C showed a linear increase with increasing temperature. However, at temperatures above 80^{o}C, we observed a decrease in the specific capacitance.

Keywords: carbon nanotubes, supercapacitor, solid state, membrane, binder-free

1 INTRODUCTION

Electrochemical energy storage devices such as batteries and electrochemical capacitors have received considerable attention due to the growing demand for energy storage solutions for automotive, renewable energy systems such as wind and solar and energy harvesting technologies[1,2]. Charge storage in electrochemical capacitors is mainly due to electrostatic double layer formation at the electrode/electrolyte interface. Electrochemical capacitors are primarily considered as a high power electrochemical device as compared to battery, which is a high energy device. Typical time constant for state-of-the-art electrochemical capacitors are in the order of seconds and are capable of storing energy density of about 5 Wh/kg. With the advent of asymmetric electrochemical capacitor design, it is now possible to improve both the cell voltage and energy density[3-5]. The improvement in power density is mainly addressed by reducing the equivalent series resistance (ESR) of the device.

The origin of ESR in electrochemical double layer capacitors (EDLCs) can be quite complex and is influenced by several factors that include contact resistance from the current collector, electronic and pore resistance of carbon electrode, binder resistance, interfacial resistance of the electrode/electrolyte and ionic resistance of the separator[6-8]. More often, the electrode resistance dominates the power performance of the capacitor and hence it is critical to design carbon materials with optimum physical properties such as porosity, surface area and electrical conductivity. In addition to electrode design, it is also important to fabricate ion conducting membranes with good electrolyte uptake, ionic conductivity and minimum interfacial resistance with the electrodes[9-11]. Electrochemical impedance spectroscopy can be a powerful tool that can be used to measure ESR and as well as throw mechanistic insights on factors that affect rate capability.

Porous activated carbons with optimum porosity in the order of 1 – 3nm and surface areas greater than 1500 m^2/g are primarily used as electrodes in EDLCs. However, due to tortuous and interconnected pore structure, the power capabilities of these electrodes are limited and typically, the relaxation frequency for capacitors made with these materials is less than 1 Hz. More recently, power capability of porous carbons has been improved by a hierarchical pore structure design but that comes with significant loss in bulk density limiting volumetric capacitance[12-14]. Carbon nanotube (CNT), due to its very high electrical conductivity can be a good electrode material for the design of high power electrochemical capacitors. CNTs can be either assembled as a buckypaper or can be directly grown on current collectors[15-24] The high power density is due to the high electrical conducitivity, mesoporosity and high electrolyte accessibility of carbon nanotubes.

In this investigation, we report for the first time the design of flexible all solid supercapacitor using high surface area ultrathin CNT paper electrodes with excellent mechanical and electrochemical properties that has a relaxation frequency of 63 Hz (time constant ~ 15 ms). In order to exploit the high power capability of CNT paper, polyvinyl alcohol (PVA) based hydrogel membranes with ionic conductivity in the order of 10^{-2} S/cm was fabricated to be used as the separator. The designed solid state

supercapacitor showed excellent cyclability (> 10000 cycles), retaining the cylability at temperatures up to 80°C.

2 EXPERIMENTAL DETAILS

2.1 Fabrication of CNT Eledtrodes

A wet chemistry post-synthesis self-assembly (PSSA) technique was used to fabricate the carbon nanotubes (CNTs) electrode. In brief, commercial CNT (Thomas Swan Elicarb) of residual noncarbonaceous content of ~ 3.5wt% was used to fabricate the electrode. First, a chlorination technique was used to digest the noncarbonaceous impurities (mostly growth catalyst) in the CNTs to improve the purity to part per million (ppm) levels. The purified CNT was dispersed and suspended in a high density liquid (Cargille Heavy Liquid) under continuous magnetic stirring for about 4 hours. The liquid was thermally evaporated slowly and was trapped cryogenically resulting in the formation of binder-free CNT electrode. The electrode was treated at high temperature to remove the remnant of the liquid. The temperature programmed oxidation (TPO) on TA Q5000IR thermogravimentric analyzer (TGA), the Renishaw InVia micro-Raman and the Micromeritic ASAP 2020 were then used to characterize the electrode.

The TPO of the commercial as-received and purified CNTs was performed at 5°C/min ramp rate from room temperature to 1000°C. The Raman spectra were collected at room temperature in the backscattering configuration using Renishaw inVia spectrometer equipped with a Peltier cooled RenCam dd-CCD. A Leica DM LM confocal microscope with 100°ø objective was used to illuminate the sample and collect the scattered light. It was set to operate at ~1 μm diameter focal spot size at the plane of the sample. A HeNe laser was used to excite the spectra, and the power at the sample was ~ 0.1mW measured using a miniature hand-held radiometer. The spectra were collected in air under ambient conditions using 514 nm wavelength laser. Both H and V polarized light were accepted in the scattered radiation. The specific surface area (SSA) of the CNT membrane was determined using the BET equation with N_2 gas at 77 K (Micromeritics ASAP 2020). The samples were degassed at 300°C under high vacuum ($P \approx 10^{-7}$ torr) for 12 h prior to measurements. To obtain pore volume and pore size distribution (PSD), the Barrett-Joyner-Holenda (BJH) model provided with the equipment with cylindrical model option was used. Total pore volume was obtained at 95% of the saturation pressure.

2.2 Synthesis of Polyvinyl alcohol (PVA) hydrogel Membrane

5g of polyvinyl alcohol (Sigma-Aldrich) was dissolved in 45 ml DI water by heating the mixture under rigorous stirring at 90°C until fully dissolved. The polymer solution was cooled down to room temperature and then 40 μL of crosslinking agent, glutaraldehyde (Sigma-Aldrich, 50 wt.% with water) was added and the mixture was stirred for 5 min. The resultant solution was then cast onto a glass plate and treated with a doctor blade to obtain an average thickness of 76 μm. The membrane was then peeled off and allowed to dry overnight at room temperature under vacuum. The dried membrane was then soaked in aqueous sulfuric acid of different concentrations for 24 hours before being used for electrochemical testing. The morphology of the membrane was characterized using Hitachi S-3500N Scanning electron microscope.

2.3 Two-Electrode Ultracapacitor

The CNT electrodes were prepared by punching out a circular disc with an area of ~1.64cm^2, and a mass of ~0.3mg measured using a Sartorius microbalance. A 500Å thin film of gold was sputtered onto CNT electrode in order to reduce interfacial contact resistance between the electrode and current collectors. Gold foil was used as the current collector for both the electrodes. Prior to the assembly of the cell, the CNT electrodes were soaked in the aqueous electrolyte for 30 minutes. The PVA membrane was also soaked in the aqueous electrolyte for 24 hours prior to assembly and dried afterward. The two-electrode symmetric capacitor was assembled together by sandwiching the current collectors, CNT electrodes and the separator.

Two-electrode capacitor characterization was performed using a Gamry Reference 3000 potentiostat/galvanostat. The cell was tested using cyclic voltammetry, electrochemical impedance spectroscopy (ESI), and constant current charge/discharge cycling. Cyclic voltammetry was done using a scan range of 0 to 1V at scan rates of 10, 50, 250, 500, 750, and 1000 mVs^{-1}. EIS measurements were performed with an AC perturbation of 10 mV at open circuit conditions. The frequency of the AC perturbation was varied from 10^5 Hz to 10^{-3} Hz. The equivalent series resistance (ESR) of the cell was computed using the impedance data measured at 1 KHz. The data was then fitted to an equivalent circuit model using Zview software. Galvanostatic charge/discharge cycling was performed by applying a load current density (based on mass of both the electrodes) ranging from 1 A/g to 50A/g for 10,000 cycles.

3 RESULTS AND DISCUSSION

Shown in Figure 1a is an optical image of a cohesive, robust, flexible, binder-free, and ultrathin freestanding CNT electrode fabricated using PSSA technique. A comparison of the Raman spectra of the commercial CNTs before purification (bottom black curve) and after purification, membrane assembly and high temperature treatment (top red curve) is shown in Figure 1b. The decrease in the D band intensity is a sign of improvement in sample quality. This is confirmed by the TGA data (Figure 1b insert) where the residual weight of the noncarbonaceous impurities decreased from 3.5wt% to below the detection limit of the TGA (<<0.1wt%). The combustion temperature increased from 563°C to 633°C ($\Delta T = 70^{o}C$).

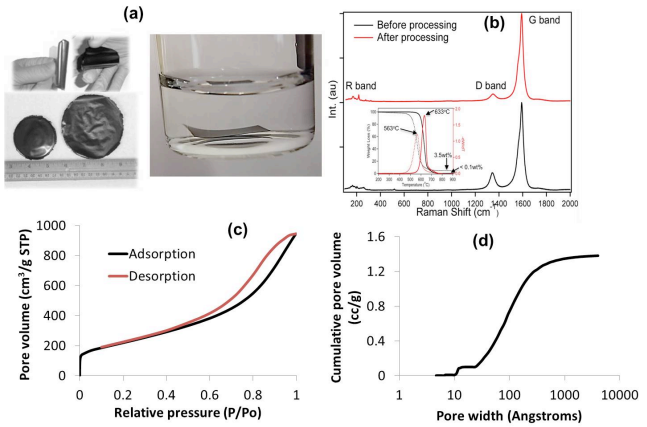

Figure 1. (a) Free standing binder free CNT electrode, (b) Raman spectra of CNT electrode before and after purification; Inset: Comparison of decomposition profile of CNT electrode (before and after purification) oxidized in air using Thermogravimetric analysis , (c) Nitrogen adsorption and desorption isotherm of CNT electrode showing presence of meso- and macropores and (d) Cumulative pore volume as a function of pore width measured using Nitrogen adsorption isotherm of CNT electrode.

Raman spectra of the membrane showed radial breathing modes (RBM) ranging from 150 cm^{-1} – 300 cm^{-1}, respectively. Based on the frequency of RBM, the diameter of the nanotubes varied from 0.8 – 1.54 nm. Figure 1c shows the nitrogen adsorption and desorption profile of SWCNT electrodes. As seen from the isotherm, there is a hysteresis at high relative pressures indicating the presence of meso- and macropores. Figure 1d shows the cumulative pore volume deduced using BJH adsorption analysis. The fabricated electrode showed a broad distribution of both mesopores (~0.1 cc/g) and a large amount of macropores ranging upto 100 nm (~1.26 cc/g). The BET surface area of the electrode was 792 m^2/g indicating the microporous nature of the electrode.

Figure 2a shows the compaction cell with the two Au leaf current collectors sticking out. The assembled flexible EDLC is shown in Figue 2b. Figure 2c is the cross-section of the PVA before the assembly and Figure 2d is the cross-section of the assembled device. After the high pressure compaction, the CNT electrodes were compressed into the polymer electrolyte as shown in the SEM image[Figure 2d]. The thicknesses of the PVA membrane and the CNT electrodes after the compaction are indicated.

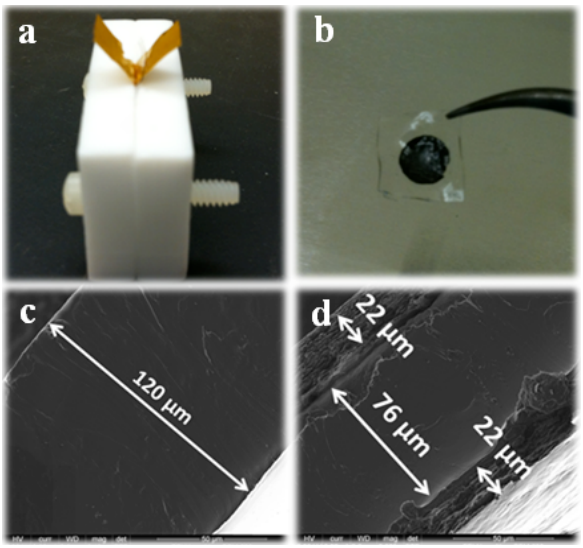

Figure 2. Optical images of (a) solid state EDLC fixed in a Teflon testing cell, (b) flexible free-standing solid state EDLC. SEM images of (c) cross section of the pure PVA/H_3PO_4 solid state electrolyte, and (d) cross-section of solid state EDLC.

The cyclic voltammetry was scanned at various rates from 50mV/s to 1000 mV/s as shown in Figure 3a. All the cyclic voltammetry curves show a fast current response on the voltage reversal at each end potential. The near-rectangular shape of the CVs illustrate a small equivalent series resistance of the CNT electrodes and rapid ionic diffusion in the solid state polymer electrolyte/separator. The specific capacitance from 20 °C to 80 °C [Fig. 2b] shows a monotonic increasing behavior with increasing temperature, consistent with electrochemical double layer mechanism in the supercapacitor. The molecular alignment of $PVA\text{-}H_3PO_4$ chains and the excitation of charge carriers with the increase in temperature might have contributed to the increase in the specific capacitance. As the temperature is increased above 80 °C, the water content in the polymer electrolyte is believed to "sweat" out, causing a decrease in the ionic conductivity. This leads to the decrease in the specific capacitance beyond 80°C [Figure 3b]. After the charge/discharge measurement at 100°C, the charge/discharge measurement was performed again at 80 °C, that showed a lower value compared to the first heating

cycle. This indicates an irreversible degradation of the polymer electrolyte at the temperature above 80 °C.

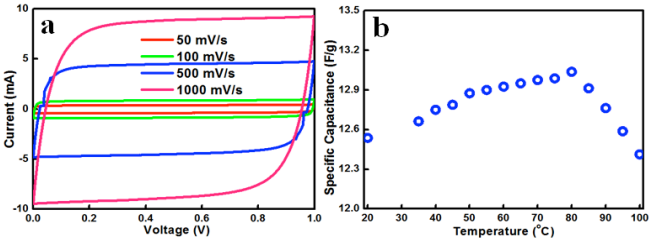

Figure 3. (a) Cyclic voltammagram at various scan rates from 50mV/s to 1000mV.s, and (b) specific capacitance as a function of temperature of a symmetric all solid state EDLC .

4 CONCLUSSION

Flexible, light-weight, and high temperature all solid state electrochemical double layer capacitor devices using polymer electrolyte and CNT electrodes have been fabricated. These devices show very high cyclability and present potential to assemble flexible all solid state bipolar supercapacitor. Systematic EIS analysis of the devices over the whole temperature range is underway to investigate the temperature effects on internal resistance and changes on the electrode/electrolyte interface.

5 AKNOWLEDGEMENTS

The authors would like to acknowledge Center for Dielectric Studies (CDS), NSF Nanosystems Engineering Research Center for Advanced Self-Powered Systems of Integrated Sensors and Technologies (ASSIST) for their financial support, Penn State Materials Research Institute and Penn State Altoona Undergraduate Research Sponsor Program.

REFERENCES

[1] Lukic, S. M.; Cao, J.; Bansal, R. C.; Rodriguez, F.; Emadi, A., *Ieee T Ind Electron* **2008,** *55*, 2258-2267.
[2] Simon, P.; Gogotsi, Y., *Nat Mater* **2008,** *7*, 845-854.
[3] Chen, H. S.; Cong, T. N.; Yang, W.; Tan, C. Q.; Li, Y. L.; Ding, Y. L., *Prog Nat Sci* **2009,** *19*, 291-312.
[4] Naoi, K., 'Nanohybrid Capacitor': *Fuel Cells* **2010,** *10*, 825-833.
[5] Xu, R.; Tang, Z. L.; Li, J. R.; Zhang, Z. T., *Prog Chem* **2009,** *21*, 235-243.
[6] Basirico, L.; Lanzara, G., *Nanotechnology* **2012,** *23*, 13-26.
[7] Portet, C.; Taberna, P. L.; Simon, P.; Flahaut, E.; Laberty-Robert, C., *Electrochim Acta* **2005,** *50*, 4174-4181.
[8] Yoon, S.; Jang, J. H.; Ka, B. H.; Oh, S. M., ss. *Electrochim Acta* **2005,** *50*, 2255-2262.
[9] Sampath, S.; Choudhury, N. A.; Shukla, A. K., *J Chem Sci* **2009,** *121*, 727-734.
[10] Kadir, M. F. Z.; Arof, A. K., *Mater Res Innov* **2011,** *15*, 217-220.
[11] Lee, P. C.; Han, T. H.; Hwang, T.; Oh, J. S.; Kim, S. J.; Kim, B. W.; Lee, Y.; Choi, H. R.; Jeoung, S. K.; Yoo, S. E.; Nam, J. D., *J Membrane Sci* **2012,** *409*, 365-370.
[12] Mi, J.; Wang, X. R.; Fan, R. J.; Qu, W. H.; Li, W. C., *Energ Fuel* **2012,** *26*, 5321-5329.
[13] Liu, N. P.; Shen, J.; Liu, D., *Micropor Mesopor Mat* **2013,** *167*, 176-181.
[14] Xing, W.; Huang, C. C.; Zhuo, S. P.; Yuan, X.; Wang, G. Q.; Hulicova-Jurcakova, D.; Yan, Z. F.; Lu, G. Q., *Carbon* **2009,** *47*, 1715-1722.
[15] Li, X.; Rong, J. P.; Wei, B. Q., *Acs Nano* **2010,** *4*, 6039-6049.
[16] Niu, C. M.; Sichel, E. K.; Hoch, R.; Moy, D.; Tennent, H., *Appl Phys Lett* **1997,** *70*, 1480-1482.
[17] An, K. H.; Kim, W. S.; Park, Y. S.; Moon, J. M.; Bae, D. J.; Lim, S. C.; Lee, Y. S.; Lee, Y. H., *Adv Funct Mater* **2001,** *11*, 387-392.
[18] Yoon, B. J.; Jeong, S. H.; Lee, K. H.; Kim, H. S.; Park, C. G.; Han, J. H., *Chem Phys Lett* **2004,** *388*, 170-174.
[19] Futaba, D. N.; Hata, K.; Yamada, T.; Hiraoka, T.; Hayamizu, Y.; Kakudate, Y.; Tanaike, O.; Hatori, H.; Yumura, M.; Iijima, S., *Nat Mater* **2006,** *5*, 987-994.
[20] Du, C. S.; Pan, N., *Nanotechnology* **2006,** *17*, 5314-5318.
[21] Du, C. S.; Pan, N., *J Power Sources* **2006,** *160*, 1487-1494.
[22] Kim, B.; Chung, H.; Kim, W., *Nanotechnology* **2012,** *23*, 8-16.
[23] Kim, B.; Chung, H.; Min, B. K.; Kim, H.; Kim, W., *Korean Chem Soc* **2010,** *31*, 3697-3702.
[24] Pan, H.; Li, J. Y.; Feng, Y. P., *Nanoscale Res Lett* **2010,** *5*, 654-668.